

THE HORIZONTAL INTERNETWORK MAGNETIC FIELD: NUMERICAL SIMULATIONS IN COMPARISON TO OBSERVATIONS WITH HINODE

O. STEINER AND R. REZAEI

Kiepenheuer-Institut für Sonnenphysik, Schöneckstrasse 6, D-79104 Freiburg, Germany

W. SCHAFFENBERGER

Physics and Astronomy Department, Michigan State University, East Lansing, MI 48824

AND

S. WEDEMEYER-BÖHM¹

Institute of Theoretical Astrophysics, P.O. Box 1029, Blindern, N-0316 Oslo, Norway

Draft version August 23, 2021

ABSTRACT

Observations with the Hinode space observatory led to the discovery of predominantly horizontal magnetic fields in the photosphere of the quiet internetwork region. Here we investigate realistic numerical simulations of the surface layers of the Sun with respect to horizontal magnetic fields and compute the corresponding polarimetric response in the Fe I 630 nm line pair. We find a local maximum in the mean strength of the horizontal field component at a height of around 500 km in the photosphere, where it surpasses the vertical component by a factor of 2.0 or 5.6, depending on the initial and boundary conditions. From the synthesized Stokes profiles we derive a mean horizontal field component that is, respectively, 1.6 and 4.3 times stronger than the vertical component. This is a consequence of both the intrinsically stronger flux density of, and the larger area occupied by the horizontal fields. We find that convective overshooting expels horizontal fields to the upper photosphere, making the Poynting flux positive in the photosphere, while this quantity is negative in the convectively unstable layer below it.

Subject headings: Sun: photosphere — Sun: magnetic fields — MHD — polarization — turbulence

1. INTRODUCTION

Recent observations with the spectropolarimeter of the Solar Optical Telescope (SOT) onboard the Hinode space observatory (Kosugi et al. 2007) indicate that the quiet internetwork region (the inner regions of supergranular cells of the quiet Sun) harbors a photospheric magnetic field whose mean flux density of the horizontal component considerably surpasses that of the vertical component (Lites et al. 2007; Orozco Suárez et al. 2007; Lites et al. 2008). According to these papers, the vertical fields are concentrated in the intergranular lanes, whereas the stronger, horizontal fields occur most commonly at the edges of the bright granules, aside from the vertical fields. In a gravitationally stratified atmosphere, vertical magnetic flux concentrations naturally develop a horizontal component as they expand with height in a funnel-like manner. Indeed, Rezaei et al. (2007) found funnel shaped magnetic elements in the internetwork from the same Hinode data. However, the newly discovered horizontal fields also occur apart from vertical flux concentrations and seem to cover a larger surface fraction than the vertical fields.

Regarding numerical simulations, Grossmann-Doerth et al. (1998), note: “we find in all simulations also strong horizontal fields above convective upflows”, and Schaffenberger et al. (2005, 2006) find frequent horizontal fields in their three-dimensional simulations, which they describe as “small-scale canopies”. Also the 3-D simulations of Abbett (2007) display “horizontally directed ribbons of magnetic flux that permeate the model chromosphere”, not unlike the figures shown

by Schaffenberger et al. (2006). More recently, Schüssler & Vögler (2008) find in a three-dimensional surface-dynamo simulation “a clear dominance of the horizontal field in the height range where the spectral lines used for the Hinode observations are formed”.

Here we report on the analysis of existing and new three-dimensional magnetohydrodynamic computer simulations of the internetwork magnetic field aiming at following questions: Does a realistic simulation of the surface layers of the Sun intrinsically produce horizontal magnetic fields and can their mean flux density indeed surpass the mean flux density of the vertical field component? What is the polarimetric signal of this field and how does it compare to measurements with Hinode?

In the following we explain in Sect. 2 the details of two simulations and present results that answer the first two of the above questions in Sect. 3. In Sect. 4, we synthesize Stokes profiles and compare them to measurements from Hinode. Conclusions follow in Sect. 5.

2. TWO SIMULATION RUNS

We have carried out two runs, run v10 and run h20, which significantly differ in their initial and boundary conditions for the magnetic field. This enables us to judge the robustness of our results with respect to magnetic boundary conditions. Both runs are carried out within a common three-dimensional computational domain extending from 1400 km below the mean surface of optical depth $\tau_c = 1$ to 1400 km above it. With this choice we ensure that the top boundary is located sufficiently high for not to unduly tamper the atmospheric layers that are in the focus of the present investigation, in particular the formation layers of the spectral lines used in polarimetric measurements with Hinode. The hori-

Electronic address: [steiner,rrezaei]@kis.uni-freiburg.de

Electronic address: schaffen@pa.msu.edu

Electronic address: sven.wedemeyer@astro.uio.no

¹ Marie Curie Intra-European Fellow of the European Commission

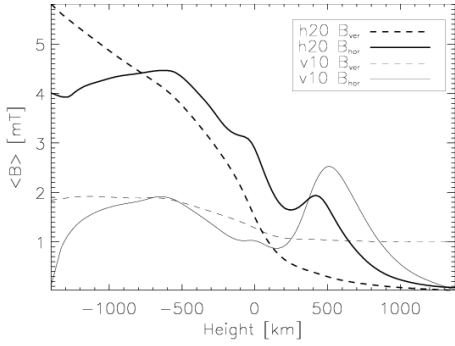


FIG. 1.— Horizontal (solid) and vertical (dashed) absolute field strength as functions of height for run h20 (heavy curves) and for run v10 (light curves).

zonal dimensions are $4\,800\text{ km} \times 4\,800\text{ km}$, corresponding to $6.6'' \times 6.6''$ on the solar disk. With 120^3 grid cells, the spatial resolution in the horizontal direction is 40 km, while in the vertical direction it is 20 km throughout the photosphere and chromosphere. Both runs have periodic lateral boundary conditions, whereas the bottom boundary is open in the sense that the fluid can freely flow in and out of the computational domain subject to vanishing total mass flux. The upper boundary is “closed”, i.e., a reflective boundary is applied to the velocity.

Run v10 starts with a homogeneous, vertical, unipolar magnetic field of a strength of 1 mT superposed on a previously computed, relaxed model of thermal convection. After relaxation, fields of mixed polarity occur throughout the photosphere with an area imbalance of typically 3:1 for fields stronger than 1 mT. The magnetic field in run v10 is constrained to have vanishing horizontal components at the top and bottom boundary but lines of force can freely move in the horizontal direction. Although this condition is quite stringent for the magnetic field near the top boundary, it still allows the field to freely expand with height through the photospheric layers. The mean vertical net magnetic flux density remains 1 mT throughout the simulation. These initial and boundary conditions might actually be more appropriate for the simulation of network magnetic fields because of preference for one polarity and the vertical direction.

Run h20 starts without a magnetic field but upwellings that enter the simulation domain across the bottom boundary area carry horizontal magnetic field of a uniform strength of 2 mT and of uniform direction parallel to the x -axis with them. Outflowing material carries whatever magnetic field it happens to have. These boundary conditions are the same as used by Stein & Nordlund (2006). They are appropriate when flux ascends from deeper layers of the convection zone, carried by convective upflows. Starting from a relaxed model of thermal convection, magnetic field steadily spreads into the convective layer of the simulation domain and after 600 s slowly begins to expand throughout the photosphere, growing in mean absolute strength. Reflective conditions apply to the field at the top boundary, resulting in $dB_{x,y}/dz = 0$, $B_z = 0$.

The magnetic energy in the box steadily increases because convective plasma motion strengthens the magnetic field. After a time of about 2.45 h an equilibrium value in magnetic energy seems to establish itself when the mean absolute vertical field strength near the surface of optical depth $\tau_c = 1$ is approximately 1 mT. Events of convective plumes pump magnetic fields in the downward direction out of the domain so that the mean Poynting flux at the lower boundary is negative, pointing out of the box.

Runs v10 and h20 have been carried out with an extended version of the computer code CO⁵BOLD² that includes magnetic fields. The code solves the coupled system of the equations of compressible ideal magnetohydrodynamics in an external gravity field taking non-local radiative transfer into account. For the present runs, frequency-independent opacities are used, which are also used for computing the continuum optical depth τ_c . The multidimensional problem is reduced to a sequence of 1-D sweeps by dimensional splitting. Each of these 1-D problems is solved with a Godunov-type finite-volume scheme using an approximate Riemann solver modified for a realistic equation of state and gravity. Details of the method can be found in Schaffenberger et al. (2005, 2006).

3. STRUCTURE AND DEVELOPMENT OF THE HORIZONTAL MAGNETIC FIELD

Figure 1 shows the horizontally and temporally averaged absolute vertical and horizontal magnetic field strength as functions of height for both runs. In run h20, the mean horizontal field strength, $\langle \sqrt{B_x^2 + B_y^2} \rangle$, is larger than the mean strength of the vertical component, $\langle |B_z| \rangle$, throughout the photosphere and the lower chromosphere: in run v10 this is the case in the height range between 250 km and 850 km. It shows a local maximum close to the classical temperature minimum at a height of around 500 km, where it is 5.6 times stronger than the mean vertical field in case of run h20. The horizontal fields also dominate in the upper photosphere of run v10 for which case one might expect the initial state and boundary condition to favor the development of vertical fields rather than horizontal ones. There, the ratio $\langle B_{\text{hor}} \rangle / \langle B_{\text{ver}} \rangle$ at the location of maximum $\langle B_{\text{hor}} \rangle$ is 2.5.

For the second half of the h20 time series and in a horizontal section at a height of mean optical depth $\tau_c = 1$, 14.2 % of the total area is covered by horizontal fields stronger than 5 mT, while this fraction is 5.1 % for the vertical fields surpassing 5 mT. At the height of 200 km in the photosphere and a threshold of 2 mT the average area fractions are 25.8 % and 6.2 %, respectively. Thus, fields with a horizontal component larger than a given limit in strength occupy a significantly larger surface area than fields with a vertical component exceeding this limit. This is a second reason (after inherent strength) why the measured mean flux density of the horizontal field component may exceed that of the vertical one.

Figure 2 (left) shows for a typical time instant in the second half of run h20 the horizontal field strength (colors) on the surface of continuum optical depth $\tau_c = 0.3$. Superimposed on the colors are contours of 2 mT of the vertical field strength, where solid and dashed contours indicate opposite polarity. To the right and the lower right of the image center, $(x, y) = (3.1, 2.5)$ and $(3.7, 1.6)$, as well as in the middle close to the front side, $(2.4, 0.3)$, we can see a frequently occurring event consisting of a “ring” of horizontal field. It starts to appear as a patch filled with horizontal field like to the left front side, $(x, y) = (0.8, 0.3)$, subsequently expanding to become a ring. The ring can also be seen in the vertical field component, where opposite halves of it have opposite polarity as is visible from the indicated 2 mT contours. This pattern arises from horizontal magnetic field that is transported to the surface by vigorous upflows. The field is anchored in the downdrafts at the edges of a granule or in the weaker upwellings of a granule interior. Here, the field is most concentrated and hence not only the vertical but also the horizontal

² www.astro.uu.se/~bf/co5bold_main.html

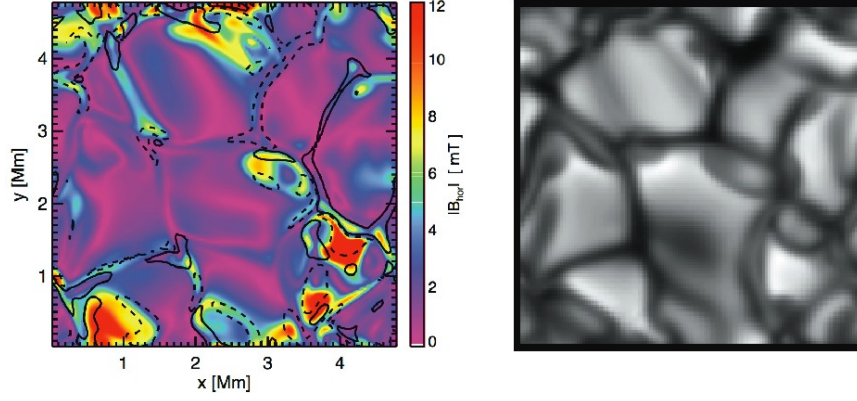


FIG. 2.— Left: Horizontal field strength on the surface of continuum optical depth $\tau_c = 0.3$. The black curves refer to contours of 2 mT vertical field strength, where solid and dashed contours have opposite polarity. Right: Map of the continuum intensity at 630 nm.

field is strongest there. As can be seen when comparing to the continuum intensity image, Figure 2 (right), a ring does often not enclose a full granule but only a part of it so that part of the vertical magnetic field occurs within the granule. The horizontal field between the crescents of vertical fields of opposite polarity covers part of the granule like a cap forming a small-scale canopy (Schaffenberger et al. 2005, 2006). Events of related topography were observed by Centeno et al. (2007) and Ishikawa et al. (2008).

As this horizontal field is pushed into the stable layers of the upper photosphere by the overshooting convection, it stops rising for lack of buoyancy, neither are there vigorous downflows that would pump it back down again. Hence, convective flow and its overshooting act to expel magnetic flux from the granule interior to its boundaries, i.e., not only to the intergranular lanes but also to the upper layers of the photosphere.

The surface of $\tau_c \approx 1$, which separates the convective regime from the subadiabatically stratified photosphere, also acts as a separatrix for the vertically directed Poynting flux, S_z , where

$$S = \frac{1}{4\pi} (\mathbf{B} \times (\mathbf{v} \times \mathbf{B})). \quad (1)$$

This can be seen in Fig. 3 (top), which displays the horizontally averaged S_z as a function of height in the atmosphere and time for the second half of run h20. The conspicuous dark streaks in the lower part of the diagram mark events of downflow plumes that carry horizontal magnetic field with them, giving rise to $\langle S_z \rangle < 0$. Differently in the photosphere, where $\langle S_z \rangle$ stays mainly positive (bright), due to the transport of horizontal fields in the upward direction. They become deposited in and give rise to the distinct layer of enhanced horizontal fields in the upper photosphere, clearly visible in the middle panel of Fig. 3. Here again, both the transport of horizontal fields downwards in the convection zone and upwards in the photosphere are visible. The bottom panel of Fig. 3 shows the mean vertical field strength that monotonically decreases with height at all times.

4. COMPARISON WITH RESULTS FROM THE HINODE SPACE OBSERVATORY

For a reality check we compare the Zeeman measurements from the Hinode spectropolarimeter with the synthesized Stokes profiles of both 630 nm Fe I spectral lines of the two simulation runs. Profiles were computed with the radiative transfer code SIR (Ruiz Cobo & del Toro Iniesta 1992; Bellot Rubio 2003) along vertical lines of sight (disk center) with a spectral sampling of 2 pm. We then applied a point

spread function (PSF) to these ‘virtual observations’: the theoretical, diffraction-limited PSF of SOT as well as two other non-ideal PSFs that take additional stray-light into account, all evaluated at $\lambda = 630$ nm (see Wedemeyer-Böhm (2008) for details). The following results refer to a PSF obtained by convolution of the ideal PSF with a Voigt function with $\gamma = 5.7'' \times 10^{-3}$ and $\sigma = 8'' \times 10^{-3}$, derived from eclipse data.

For a faithful comparison with the results of Lites et al. (2008), we subject the synthetic profiles to the same procedure for conversion to apparent flux density³ as was done by these authors. Thus, we obtain calibration curves for the conversion from the wavelength integrated polarization signals V_{tot} and Q_{tot} to the apparent longitudinal and transversal magnetic flux densities $|B_{\text{app}}^L|$ and B_{app}^T , respectively. Equally, Q_{tot} is the resulting Q -profile after transformation to the ‘preferred-frame azimuth’ in which the $+Q$ -direction is parallel to the projection of the magnetic field vector on the plane of sky, when $U \approx 0$.

Having the calibration curves, we derive spatial and temporal averages for the transversal and longitudinal apparent magnetic flux densities, B_{app}^T and $|B_{\text{app}}^L|$ of respectively 21.5 Mx cm^{-2} and 5.0 Mx cm^{-2} for the second half of run h20 and 10.4 Mx cm^{-2} and 6.6 Mx cm^{-2} for run v10. Thus, the ratio $r = \langle B_{\text{app}}^T \rangle / \langle |B_{\text{app}}^L| \rangle = 4.3$ in case of run h20 and 1.6 in case of run v10. Lites et al. (2008) obtain from Hinode SP data $\langle |B_{\text{app}}^T| \rangle = 55 \text{ Mx cm}^{-2}$ and $\langle |B_{\text{app}}^L| \rangle = 11 \text{ Mx cm}^{-2}$ resulting in $r = 5.0$.

While $\langle B_{\text{hor}} \rangle / \langle B_{\text{ver}} \rangle = 5.6$ and 2.5 for run h20 and v10, respectively, at the location of maximum $\langle B_{\text{hor}} \rangle$, the above quoted lower ratios result because the main contribution to the Stokes signals does not come from this height but rather from the low photosphere, where the two components differ less (see Fig. 1). At full spatial resolution, i.e., without application of the PSF, we obtain from the synthesized Stokes data of run h20 $B^T = 24.8 \text{ Mx cm}^{-2}$ and $|B^L| = 8.8 \text{ Mx cm}^{-2}$, thus $r = 2.8$. The higher ratio r when applying the PSF results because of apparent flux cancellation within a finite resolution element. The vertical component is more subject to this effect than the horizontal one because of its smaller spatial scale and higher intermittency. This indicates that the predominance of the horizontal component decreases with increasing spatial resolution and that spatial resolution is a fundamental parameter to take into account when interpreting measurements of

³ Apparent because finite spatial resolution may mask the true flux density through cancellation of opposite polarization.

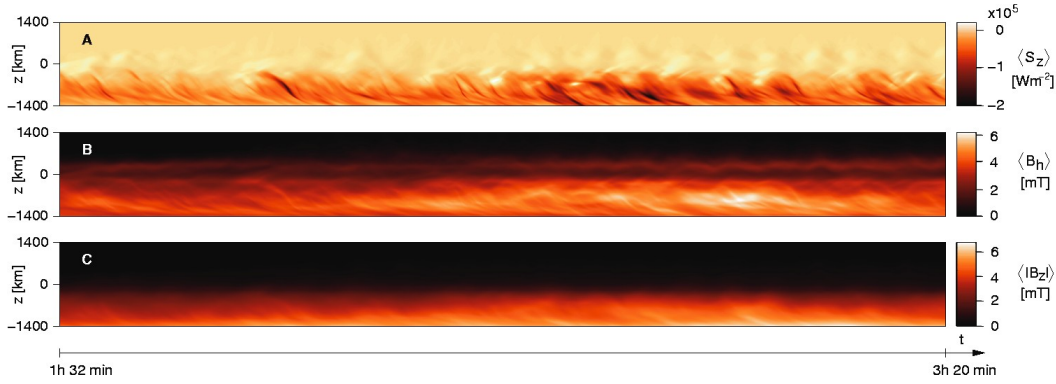


FIG. 3.— Vertically directed Poynting flux, S_z , horizontal magnetic flux density, $\langle B_h \rangle$, and vertical absolute magnetic flux density, $\langle |B_z| \rangle$ as functions of height and time from run h20. All quantities are averages in horizontal planes of the three-dimensional computational box. The temporal average of $\langle S_z \rangle$ is maximal $7.4 \times 10^2 \text{ Wm}^{-2}$ (at 200 km) and minimal $-5.2 \times 10^4 \text{ Wm}^{-2}$ (at -800 km).

field inclinations (Orozco Suárez et al. 2007). The probability density for the field inclination at full spatial resolution of the simulation shows on the surface $\tau_c = 0.01$ a flat (isotropic) distribution in the range $\pm 50^\circ$ from the horizontal direction.

5. CONCLUSIONS

We have carried out two simulations of magnetoconvection in the surface layers of the quiet internetwork region of the solar atmosphere. The simulations greatly differ in their initial state and boundary conditions for the magnetic field, but otherwise they both equal faithfully reproduce properties of normal granulation (as the magnetic field is weak). The top boundary is placed in the middle chromosphere (at a height of 1400 km) far away from the photospheric layers.

Both simulations intrinsically produce a horizontal magnetic field throughout the photosphere and lower chromosphere with a mean field strength that exceeds the mean strength of the vertical field component at the same height by up to a factor of 5.6. The strength of the horizontal field component shows a local maximum close to the classical temperature minimum near 500 km height (which largely escapes measurements with the Fe I 630 nm line pair). Fields with a horizontal component exceeding a certain limit in strength occupy a significantly larger surface area than fields with a vertical component exceeding this limit.

This horizontal field can be considered a consequence of the flux expulsion process (Galloway & Weiss 1981): in the same way as magnetic flux is expelled from the granular interior to the intergranular lanes, it also gets pushed to the middle and upper photosphere by overshooting convection, where it tends

to form a layer of horizontal field of enhanced flux density, reaching up into the lower chromosphere. Below the surface of $\tau_c \approx 0.1$, convective plumes pump horizontal magnetic field in the downward direction. Hence, this surface acts as a separatrix for the Poynting flux, which is mainly directed upwards above it and in the downward direction below it.

The response of this field in linear and circular polarization of the two neutral iron lines at 630 nm yields a ratio $\langle B_{\text{app}}^T \rangle / \langle |B_{\text{app}}^L| \rangle = 4.3$ in case of run h20 (which, according to Sect. 2, we deem better to represent the conditions of internetwork regions). This is close to the measurements of Lites et al. (2008), which indicate a factor of 5. Errors may come from the straylight produced by the spectrograph and polarization optics that was not taken into account with our PSF, the difference in mean absolute flux density (run h20, has only about half the measured value [see Sect. 4]), the frequency-independent treatment of radiative transfer, lacking spatial resolution, but also natural fluctuations. The predominance of the horizontal component, may possibly only exist on a scale comparable to or less than the spatial resolution of SOT. At full spatial resolution of the simulation we obtain a ratio of 2.8 instead of 4.3.

The authors thank B.W. Lites for providing the calibration software, R. Hammer and M. Schüssler for detailed comments on a draft version of this paper, and L.R. Bellot Rubio for helping greatly improving it. This work was supported by the Deutsche Forschungsgemeinschaft (SCHM 1168/8-1).

REFERENCES

- Abbett, W. P. 2007, *ApJ*, 665, 1469
- Bellot Rubio, L. R. 2003, Inversion of Stokes profiles with SIR, (Freiburg: Kiepenheuer Institut für Sonnenphysik)
- Centeno, R., Socas-Navarro, H., Lites, B., Kubo, M., Frank, Z., Shine, R., Tarbell, T., Title, A., Ichimoto, K., Tsuneta, S., Katsukawa, Y., Suematsu, Y., Shimizu, T., & Nagata, S. 2007, *ApJ*, 666, L137
- Galloway, D. J., & Weiss, N. O. 1981, *ApJ*, 243, 945
- Grossmann-Doerth, U., Schüssler, M., & Steiner, O. 1998, *A&A*, 337, 928
- Ishikawa, R., Tsuneta, S., Ichimoto, K., Isobe, H., Katsukawa, Y., Lites, B. W., Nagata, S., Shimizu, T., Shine, R. A., Suematsu, Y., Tarbell, T. D., & Title, A. M. 2008, *A&A*, 481, L25
- Kosugi, T., Matsuzaki, K., Sakao, T., Shimizu, T., Sone, Y., Tachikawa, S., Hashimoto, T., Minesugi, K., Ohnishi, A., Yamada, T., Tsuneta, S., Hara, H., Ichimoto, K., Suematsu, Y., Shimojo, M., Watanabe, T., Shimada, S., Davis, J. M., Hill, L. D., Owens, J. K., Title, A. M., Culhane, J. L., Harra, L. K., Doschek, G. A., & Golub, L. 2007, *Sol. Phys.*, 243, 3
- Lites, B. W., Kubo, M., Socas-Navarro, H., Berger, T., Frank, Z., Shine, R., Tarbell, T., Title, A., Ichimoto, K., Katsukawa, Y., Tsuneta, S., Suematsu, Y., Shimizu, T., & Nagata, S. 2008, *ApJ*, 672, 1237
- Lites, B. W., Socas-Navarro, H., Kubo, M., Berger, T., Frank, Z., Shine, R., Tarbell, T., Title, A., Ichimoto, K., Katsukawa, Y., Tsuneta, S., Suematsu, Y., Shimizu, T., & Nagata, S. 2007, *PASJ*, 59, 571
- Orozco Suárez, D., Bellot Rubio, L. R., del Toro Iniesta, J. C., Tsuneta, S., Lites, B. W., Ichimoto, K., Katsukawa, Y., Nagata, S., Shimizu, T., Shine, R. A., Suematsu, Y., Tarbell, T. D., & Title, A. M. 2007, *ApJ*, 670, L61
- Rezaei, R., Steiner, O., Wedemeyer-Böhm, S., Schlichenmaier, R., Schmidt, W., & Lites, B. W. 2007, *A&A*, 476, L33
- Ruiz Cobo, B., & del Toro Iniesta, J. C. 1992, *ApJ*, 398, 375
- Schaffnerberger, W., Wedemeyer-Böhm, S., Steiner, O., & Freytag, B. 2005, in *ESA Special Publication*, Vol. 596, *Chromospheric and Coronal Magnetic Fields*, ed. D. E. Innes, A. Lagg, & S. A. Solanki
- Schaffnerberger, W., Wedemeyer-Böhm, S., Steiner, O., & Freytag, B. 2006, in *ASP Conference Series*, Vol. 354, *Solar MHD Theory and Observations*, ed. J. Leibacher, R. F. Stein, & H. Uitenbroek, 345
- Schüssler, M., & Vögler, A. 2008, *A&A*, 481, L5
- Stein, R. F., & Nordlund, Å. 2006, *ApJ*, 642, 1246
- Wedemeyer-Böhm, S. 2008, Point spread functions for the Solar Optical Telescope onboard Hinode, *ArXiv e-prints* 0804.4536, *A&A*, 804